Optical imaging for brain tissue characterization using relative fluorescence lifetime imaging

Asael Papour
Zach Taylor
Adria Sherman
Desiree Sanchez
Gregory Lucey
Linda Liau
Oscar Stafsudd
William Yong
Warren Grundfest

Optical imaging for brain tissue characterization using relative fluorescence lifetime imaging

Asael Papour,[a] **Zach Taylor,**[b] **Adria Sherman,**[b]
Desiree Sanchez,[c] **Gregory Lucey,**[c] **Linda Liau,**[d]
Oscar Stafsudd,[a] **William Yong,**[c] **and**
Warren Grundfest[a,b]
[a]University of California Los Angeles, Department of Electrical Engineering, Los Angeles, California 90095
[b]University of California Los Angeles, Department of Bioengineering, 410 Westwood Plaza, Room 5121, Engineering V, P.O. Box 951600, Los Angeles, California 90095-1600
[c]University of California Los Angeles, Brain Tumor Translational Resource, Los Angeles, California 90095
[d]University of California Los Angeles, Department of Neurosurgery, Los Angeles, California 90095

Abstract. An autofluorescence lifetime wide-field imaging system that can generate contrast in underlying tissue structures of normal and malignant brain tissue samples with video rate acquisition and processing time is presented. Images of the investigated tissues were acquired with high resolution ($\sim$35 μm) using an algorithm to produce contrast based on differences in relative lifetimes. Sufficient contrast for delineation was produced without the computation of fluorescence decay times or Laguerre coefficients. The imaged tissues were sent for histological analysis that confirmed the detected imaged tissues morphological findings and correlations between relative lifetime maps and histology identified. © 2013 Society of Photo-Optical Instrumentation Engineers (SPIE) [DOI: 10.1117/1.JBO.18.6.060504]

Fluorescence lifetime imaging has demonstrated the ability to accurately detect materials and tissue constituents with robustness to varying yield and emission scattering materials.[1–6] Current fluorescence lifetime systems rely on accurate temporal sampling to capture the tails of the decaying emission. These data are often fit to an exponential decay model or a set of Laguerre polynomials to extract coefficients related to decay times.[5–9] Although these methodologies provide powerful tools for material constituent identification, they are often implemented as point measurement systems and require significant postprocessing to compute decay times and/or coefficients. In some applications these factors can hinder clinical translation.

Based on these observations, our group has developed algorithms and system designs that trade away information (explicit extraction of decay times) for improvements to system simplicity and image acquisition time. Contrast is generated by developing spatially resolved maps of relative differences in auto-fluorescence decay of tissue constituents. This method uses a gated charge-coupled device (CCD) and diode array and was explored in a previously published paper,[1] and the pertinent details are repeated below. The system has accomplished fast acquisition and processing algorithms that allow for a wide field to be acquired simultaneously and may extend the use of this modality to the intraoperative environment.[1] These improvements were enabled by employing light emitting diodes (LED) and long illumination pulse durations to create a detection system capable of imaging a wide field of view (FOV) with high resolution while maintaining low peak power and avoiding photo bleaching (Fig. 1). The resulting image displays a map proportional to the relative lifetime values on a predetermined color scale. This approach ensures very fast processing since only two images are acquired and no deconvolution or lifetime calculations are needed. The system has demonstrated an ability to distinguish between lifetime differences of less than 6% in imaging dyes and powders.[1] We show here for the first time the utility of the system in distinguishing brain tissue morphology and structure followed by histological analysis confirming the contrast mechanism and sensitivity of the system.

This current iteration has undergone numerous upgrades to increase the contrast and ease of operability. Illumination has been modified to a circular aperture mounted with six ultraviolet (UV)-LEDs to ensure more uniformity when imaging rough surfaces. Each LED is rated at 2 mW optical power at 375 nm central wavelength. The LEDs' circuit operates at an average optical power of 2 μW driven by a high-voltage pulse generator (Avtech AVR-E2-C) at 0.02% duty cycle. The low-duty cycle ensures thermal stability of the LEDs and produces fluence levels at five orders of magnitude below the ANSI standard [Z136.1_2007]. A filter mount has been placed in front of the intensified CCD (iCCD) (AndoriStar DH734) to take advantage of the wavelength-dependent decay times of tissue constituents. The imaging optic utilized in this experiment was a high-numerical aperture SLR macro lens (Canon MP-E 65) which afforded a $\sim$1-cm FOV at a standoff of $\sim$8 cm. With these specifications and the iCCD camera's focal plane array dimensions, the practical feature size limit is $\sim$35 μm.

A diagram of the operational principles of the algorithm is displayed in Fig. 2. The comprehensive acquisition method has been described in Jiang et al. and a concise summary is described here; the gated intensified camera is set to capture two images, one during the illumination period and the other during the fluorescence decay period. These two images contain all the information needed to discern between different constituents and eliminate varying yield factors and absorption while being sensitive only to lifetime differences (Fig. 2). Each pixel is normalized to its maximum fluorescence emission (in the calibration image), and hence yield and absorbance do not interfere with lifetime information representation. Software execution of this algorithm involves the pixel-wise division of two 1M pixels images in a 16-bit format, and requires a processing time of $\sim$5 ms using MATLAB without any optimizations. Moreover, using this long acquisition method ensures signal to noise ratio (SNR) is not the limiting factor for the generation of sufficient contrast and allows a total acquisition of 1 s. Typical

Address all correspondence to: Warren Grundfest, University of California Los Angeles, Department of Bioengineering, 410 Westwood Plaza, Room 5121, Engineering V, P.O. Box 951600, Los Angeles, California 90095-1600. Tel: 310-794-5550; Fax: 310-794-5956; E-mail: warrenbe@seas.ucla.edu
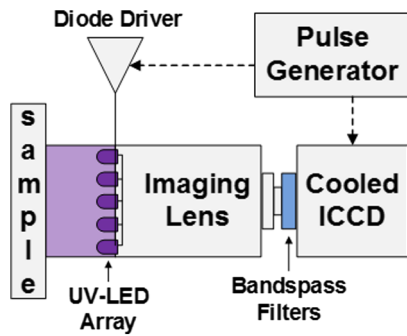
Fig. 1 Schematics of the fluorescence acquisition system. The optical pulse and the camera gate are synchronized and detailed in Ref. 1.

pulse width is in the order of 10 ns, while the detection gap between the two acquisitions is system dependent and being investigated in ongoing research.

Brain tissue samples were selected to test the capabilities of this system to delineate varying tissue pathologies. One frozen glioma sample and one frozen dura mater sample were acquired from the UCLA Brain Tumor Translational Resource (BTTR) and placed on glass microscope slides for imaging. The glioma tissue was from a histologically confirmed glioblastoma WHO Grade IV patient, though the sample used for this study showed only infiltrating areas of the glioma without necrosis. The tissue was mounted in optical coherence tomography and then sliced flat with a cryotome to ensure a flat imaging field. The samples were placed on a cooled stage with a temperature controlled thermoelectric cooler to slow the deterioration of tissue at room temperature. Following acquisition, the samples were marked with a standard histology dye for orientation purposes and sent to the BTTR for histological analysis.
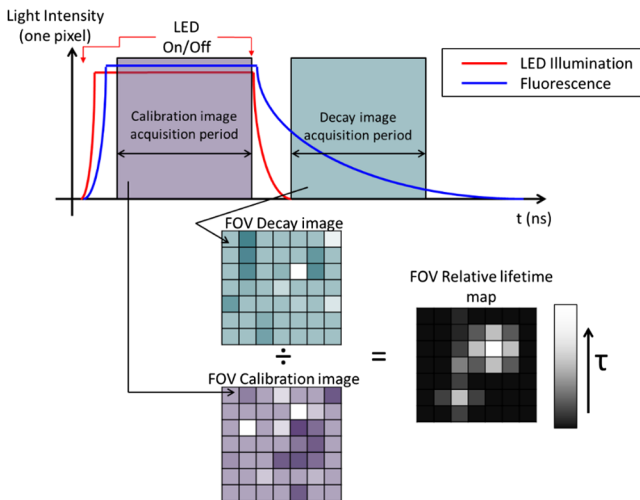
Fig. 2 Relative fluorescent lifetime algorithm. Acquisition methodology: a calibration image is acquired during LED illumination and then saved, CCD resets and the second image – the decay image – is acquired and saved. The decay image is then divided by the calibration image: each pixel's intensity value in the decay image is divided with the corresponding pixel in the calibration image; this results in a final relative lifetime image (normalized image). Each pixel is integrating the intensity of the fluorescence signal during the acquisition period, hence the advantage of high SNR in our system. Since the fluorophore lifetime and recorded signals are correlated, this algorithm presents only the relative lifetime information, where bright pixels represent longer lifetimes.
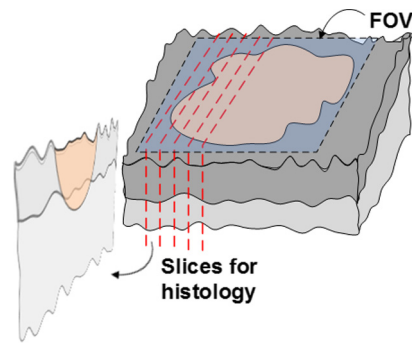

Fig. 3 The bread slice loafing employed by the BTTR. This method ensures relevant histological analysis with corresponding imaging results. Samples are sectioned vertically to the imaging plane, acquiring depth information, thus achieving full histopathological characterization that we correlate to imaging.

The preparation of the samples for histological analysis included embedding in paraffin while maintaining the desired orientation. In order to obtain maximum information of the tissue surface while maintaining orientation, the samples were sliced vertically, similar to bread slicing as illustrated in Fig. 3, and stained with hematoxylin and eosin prior to mounting on a slide for microscopy.

Since our system has a large sensitivity range (1-MHz readout with 13 bit effective dynamic range), good visual contrast is hard to perceive even on modern LCD screens, however, customization of the image lookup table can mediate that problem [Fig. 4(c) and 4(d)]. Choosing an optimized color map (lookup table) to represent relative lifetime values with even higher apparent contrast is being optimized by our group and others.[10] Figure 4 displays gray scale fluorescence intensity (steady state) images of the glioma sample [Fig. 4(a)] and dura mater [Fig. 4(b)]—high intensity corresponds to brighter pixels. The lifetime images in Fig. 4(c) and 4(d) are displayed with the color map adjacent to each image, where shorter relative lifetimes are yellow (and blue) and longer relative lifetimes are red.

These lifetime images display contrast that is not detectable in the gray scale "calibration" images Fig. 4(a) and 4(b) and show ine structure corresponding to tissue morphology. Figure 4(e) shows a low to moderate cellularity area of neoplastic astrocytes from a glioblastoma patient. The histology of region I is fairly uniform which correlates well with the relative uniformity of the lifetime fluorescence image. Figure 4(f) and 4(g) shows histology from two distinct regions of a sample of dura mater. Region I is a relatively cellular area showing multiple nuclei. Region II was relatively devoid of fibroblastic nuclei and consisted mostly of dense collagen. Pathological results correlate with the relative lifetime map and further confirm the system's ability to detect tissue abnormalities. The heterogeneous imaging signals arising from regions I and II may reflect the relative presence or absence of fibroblasts in these areas.

Using relative lifetime normalization methodology to create contrast images has great potential when used in *ex vivo* samples. The rapid imaging rate and the high contrast generated offer a unique implementation of fluorescence lifetime imaging that carries the potential for intraoperative cancer margin delineation and accurate scission that offers better patient outcome. Those capabilities coupled with modular, low cost components, bring closer the realization to implement this system in a clinical
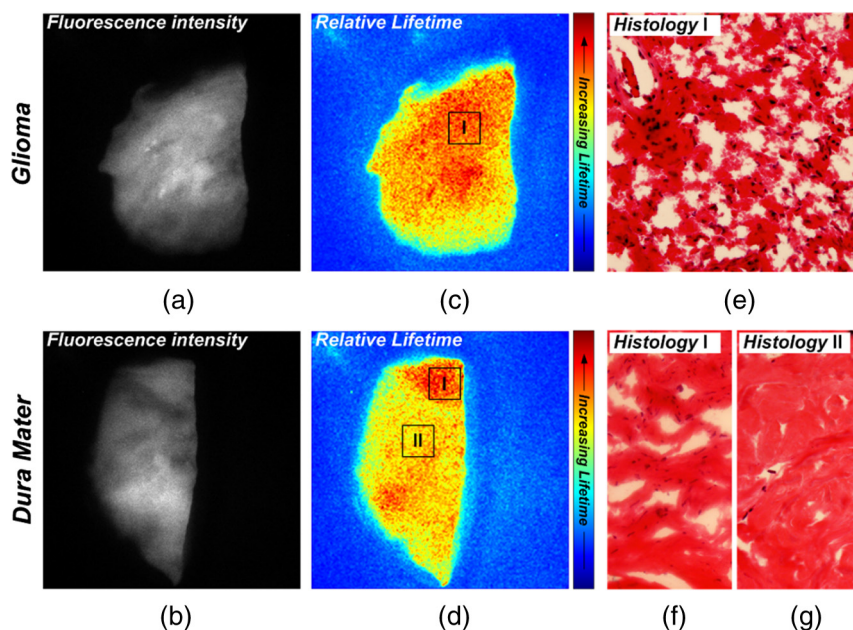
Fig. 4 Brain tissue results and analysis. (a) and (b) Fluorescence intensity images of the "calibration image." (c) and (d) Custom color map of relative lifetimes: red represents longer lifetime. (e) Histology results of the marked region in (c) showing malignant tissue composition; glioma tissue was relatively uniform hence only one area was tested. (f) and (g) Histology results of regions I and II, respectively, marked in (d). The relative lifetime map was not altered or enhanced other than applying the color map to pixel's values.

setting. Further research with a large sample pool to generate significant statistical data is underway.

References

1. P.-C. Jiang, W. S. Grundfest, and O. M. Stafsudd, "Quasi-real-time fluorescence imaging with lifetime dependent contrast," *J. Biomed. Opt.* **16**(8), 086001 (2011).
2. J. Phipps et al., "Fluorescence lifetime imaging for the characterization of the biochemical composition of atherosclerotic plaques," *J. Biomed. Opt.* **16**(9), 096018 (2011).
3. J. E. Phipps, Y. Sun, M. C. Fishbein, and L. Marcu, "A fluorescence lifetime imaging classification method to investigate the collagen to lipid ratio in fibrous caps of atherosclerotic plaque," *Lasers Surg. Med.* **44**(7), 564–571 (2012).
4. Y. Sun et al., "Fluorescence lifetime imaging microscopy for brain tumor image-guided surgery," *J. Biomed. Opt.* **15**(5), 056022 (2010).
5. J. McGinty et al., "Wide-field fluorescence lifetime imaging of cancer," *Biomed. Opt. Exp.* **1**(2), 627–640 (2010).
6. J.-M. I. Maarek et al., "Time-resolved fluorescence spectra of arterial fluorescent compounds: reconstruction with the Laguerre expansion technique," *Photochem. Photobiol.* **71**(2), 178–187 (2000).
7. J. A. Jo, Q. Fang, and L. Marcu, "Ultrafast method for the analysis of fluorescence lifetime imaging microscopy data based on the Laguerre expansion technique," *IEEE J. Quantum Electron.* **11**(4), 835–845 (2005).
8. C. J. de Grauw and H. C. Gerritsen, "Multiple time-gate module for fluorescence lifetime imaging," *Appl. Spectrosc.* **55**(6), 670–678 (2001).
9. N. P. Galletly et al., "Fluorescence lifetime imaging distinguishes basal cell carcinoma from surrounding uninvolved skin," *Br. J. Dermatol.* **159**(1), 152–161 (2008).
10. C. Stringari et al., "Phasor approach to fluorescence lifetime microscopy distinguishes different metabolic states of germ cells in a live tissue," *Proc. Natl. Acad. Sci.* **108**(33), 13582–13587 (2011).